Computer Analysis of Kinematic Parameters of the Intact Heart Using X-ray Image Sequence

(X-ray 影像을 利用한 心臟運動解析에 關한 硏究)

閔 丙 九*, 金 性 完**, 金 喜 贊**

(Byoung Goo Min, Sung Wan Kim, and Hee Chan Kim)

要 約

움직이는 물체의 영상으로부터 그 물체의 운동을 해석하는 것은 매우 중요하다. 본 논문에서는 X-ray 영상을 이용하여 심장운동을 해석하는 알고리즘에 관하여 연구하였다.

관상동맥 혈관조영상을 이용하여 심장운동에 따른 국부적인 심근표면(Epicardial)의 변형과 심근두께의 변화 그리고 이에 작용하는 원주 방향 및 길이 방향의 응력을 추정하는 새로운 수학적인 방법을 개발하였다. 이 새로운 방법에서는 관상동맥의 분지점 영상의 시간에 따른 위치 변화를 심장운동 해석의 기본 data로 사용하였다.

4마리 개와 1사람의 관상동맥 조영상을 이용한 실제 실험결과로 부터 본 논문의 방법이 납으로 만든 marker를 붙여 얻은 결과와 비교하여 볼때 타당성이 있음을 알 수 있었다.

따라서 이 방법을 이용하면 관상동맥 혈관조영상으로 부터 기존의 혈관상태에 관한 정보 이외에도 국부 심근운동에 따른 변형 및 응력(stress)을 얻을 수 있게 된다.

Abstract

It is important to extract the mechanical informations from the image sequences of the moving object. We have studied the computer algorithms for analysis of the moving heart using X-ray image sequence.

A new mathematical method was developed to estimate the local epicardial deformation, wall thickness, and the regional circumferential and longitudinal wall strees using biplane coronary cineangiograms. In this method, the motion images of the coronary artery bifurcation points were used as natural landmarks for the kinematic analysis of the ventricular deformation. In four dogs and a normal patient's coronary cineangiograms, the estimation results show the validity of the present analysis, compared with the experimental results based upon the implanted markers. Thus, the present method provides a new method of evaluating the regional wall deformation and wall stress together with the blood vessel conditions using the coronary cineangiography procedure.

*正會員, 서울大學校 醫科大學 醫工學科

(Dept. of Biomedical Eng., Seoul National Univ.)

**準會員, 서울大學校 工科大學 制御計則 工學科

(Dept. of Control and Instrumentain Eng., Seoul National Univ.)

接受日字 : 1985年 4月 2日

I. INTRODUCTION

The regional changes of cardiac wall deformation and the wall stress are important for evaluation of the myocardial functions. However, their application for clinical diagnosis

has been limited, because it is difficult to measure these regional myocardial parameters in the intact heart.

Meier et al.[1] and Walley et al.[2] used the radiographic images of the implanted radiopaque markers in the beating heart to estimate the local twist and segmental shortening of small epicardial segment.

After elimination of the effects of the time-varying displacements of the overall cardiac motion using kinematic approaches, the local deformation was represented by the regional rotation tensor and the muscle wall stretch tensor. Also, the changes of wall thickness could be computed from the stretch tensor under the assumption of the isochoric deformation.

While the regional wall stress is known also as one important contractile parameter of the muscle fiber in normal and abnormal cardiac functions, it has been difficult to measure the regional changes of wall stress. Sandler and Dodge [7] studied the average stresses for an ellipsoidal model with finite wall thickness based upon Laplace's law[8]. Wong and Rautaharju[9] estimated the stress distribution including the effects of shear and bending moments, which were shown to be negligible by Mirsky[10].

In the present study, we evaluated whether the motion images of the coronary bifurcation points can be used for computation of the local deformation and the regional wall stress, thus avoiding thoracotomic procedures for implantation of markers. The local wall deformation and the regional wall stress were computed using the kinematic method of three feature points around the coronary bifurcation points.

This method of utilizing the moving coronary bifurcation points as natural markers can increase the usefulness of the coronary cineangiography by providing the regional myocardial status in addition to the vessel's patency.

Usage of the coronary artery bifurcations for determination of the global epicardial displacements was previously investigated by Kong et al.[3] and Potel et al.[4]. Kong's results showed a close coorelation between the spacial changes of bifurcations' interdistances and the implanted markers' displacements during a heart cycle. This result provided a basis of using the displacement data of the bifurcation points for computation of the cardiac wall thickness and the wall stress in the intact heart.

II. ANALYSIS

A. Representation of Regional Myocardial Motion.

It has been shown [1] that the regional cardiac wall deformation can be approximated as homogeneous changes, and described by a linear tensor of gradient, T, in a small myocardial region. This deformation tensor, T, related the position data of feature points in the reference frame of the end-diastolic phase to those in the following sequential frames within a heart cycle. Also, this deformation tensor can be uniquely represented by the product of the orthonormal rotation tensor, R, and the positive symmetric stretch tensor, D, using a polar decomposition theorem [1],

$$T = R \cdot D \tag{1}$$

Therefore, when the instantaneous deformation tensor is calculated from the position data of the feature points, one can evaluate the numerical values of the tensors R and D uniquely. The tensor, R, provides a rotation angle, α, and the eigenvalues of the stretch tensor, D, provides the epicardial strains and the tensor's eigenvectors show the principal shortening axes of the deformation.

B. Local Myocardial Coordinate System.

The global effects of heart motion by translation, rotation, and torsion should be eliminated before analyzing the regional epicardial motion. In Meier et al.'s method, these overall motion effects were eliminated by the coordinate transformation method using the position data of the ventricular apex and the base. Since these position data are difficult to obtain for the same heart cycle in the coronary angiograms, however, we

used the following approach based upon the simplified perspective coordinate transformation [5].

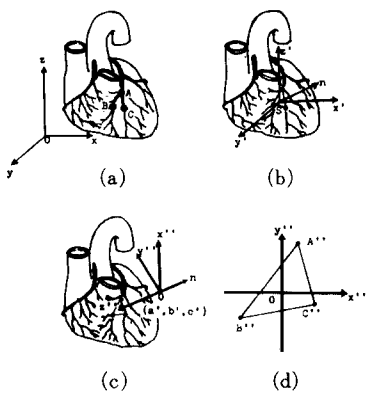

Fig. 1. Schematic diagram of the coordinate system transformation procedure for the elimination of the global heart motion;
(a) external camera coordination system (x,y,z) and three feature points A,B, C,
(b) translated coordinate system (x', y', z') with its origin located at the centroid points S, and
(c) observer coordinate system (x", y", z") with its origin on the normal vector component, n', of the $\triangle$ABC.
(d) The moving position data of the feature points are represented by two-dimensional data, A", B", C", after transformation.

In a small triangular plane composed of three feature points A,B,C located on the coronary arterial tree, as shown in Fig. 1(a), the time-varying centroid point, S, of the triangle ABC is computed in the external coordinate basis (x,y,z) during a heart cycle as follows;

$$S(t) = A(t) + B(t) + C(t) / 3 \qquad (2)$$

Since this centroid point moves together with the heart, the effects of global translation can be eliminated in a new coordinate system (x', y', z') with its origin located at the centroid point.

In the new coordinate system, three feature points A,B,C are represented as follow in Fig. 1(b),

$$\begin{aligned} A'(t) &= A(t) - S(t) \\ B'(t) &= B(t) - S(t) \\ C'(t) &= C(t) - S(t). \end{aligned} \qquad (3)$$

Then, we can use the simplified perspective transformation method to transform the (x', y', z') coordinate system to the observer coordinate system (x", y", z") where the z" axis is on the normal vector component, n', of the triangular plane ABC, as shown in Fig. 1(c). These transformation can be expressed as follows, using a homogeneous coordinate representation [5].

$$[x'', y'', z'', 1] = [x', y', z', 1] \times \begin{bmatrix} \frac{-b'}{R_2} & \frac{-a'c'}{R_1 R_2} & \frac{-a'}{R_1} & 0 \\ \frac{a'}{R_2} & \frac{-b'c'}{R_1 R_2} & \frac{-b'}{R_1} & 0 \\ 0 & \frac{R_2}{R_1} & \frac{-c'}{R_1} & 0 \\ 0 & 0 & R_1 & 1 \end{bmatrix} \qquad (4)$$

and $n'(t) = \{C(t) - B'(t)\} \times \{A'(t) - B'(t)\}$,

where (a', b', c') is an arbitrary viewing point on the normal vector n'(t) in the (x',y',z') coordinate system,

$$R_1 = (a'^2 + b'^2 + c'^2)^{1/2}$$

and $R_2 = (a'^2 + b'^2)^{1/2}$

If the viewing position (a', b', c') has a fixed distance from the centroid, the z" axis data will always have constant values of R_1 after the above perspective transformation. Then, the moving position data of the feature points can be represented by the two-dimensional values, as shown in Fig. 1(d).

C. Local Epicardial Deformation and Strains

As the reference frame of the deformation tensor, T, is given at the end-diastolic phase, this tensor describes the time-varying ventricular deformation during a heart cycle relative to its end-diastolic shape and orientation. In

this case, the matrix of the position data of three feature points, W(t), can be expressed in the observer coordinate (x'', y'', z'') as follows;

$$W(t) = T(t) \cdot Wed, \tag{5}$$

where

$$W(t) = \left[A''(t) \mid B''(t) \mid C''(t) \right] = \begin{bmatrix} A_x''(t) & B_x''(t) & C_x''(t) \\ A_y''(t) & B_y''(t) & C_y''(t) \\ R_1 & R_1 & R_1 \end{bmatrix}$$

$$W_{ed} = \left[A_{ed}'' \; B_{ed}'' \; C_{ed}'' \right],$$

and A_{ed}'', B_{ed}'', C_{ed}'' are the observer coordinate's position data of three feature points at the end-diastolic phase. From Eq. (5), the deformation tensor, T, can be computed using the least squares estimation technique as follows[2],

$$\hat{T}(t) = W(t) \cdot W_{ed}^{T} \cdot (W_{ed} \cdot W_{ed}^{T})^{-1} \tag{6}$$

Then, $\hat{T}(t)$ can be uniquely represented by the product of the R and D in Eq.(1), [1]

$$\hat{T}(t) = R(t) \cdot D(t) \tag{7}$$

$$\text{or} \begin{bmatrix} \hat{T}_{11}(t) & \hat{T}_{12}(t) \\ \hat{T}_{21}(t) & \hat{T}_{22}(t) \end{bmatrix} = \begin{bmatrix} \cos\alpha(t) & -\sin\alpha(t) \\ \sin\alpha(t) & \cos\alpha(t) \end{bmatrix} \times \begin{bmatrix} D_{11}(t) & D_{12}(t) \\ D_{12}(t) & D_{22}(t) \end{bmatrix},$$

where $\alpha(t)$ is the local twist angle.

By solving the above simultaneous equations, one can obtain the numerical values of the rotation tensor, R(t), and the stretch tensor, D(t), from the estimated tensor $\hat{T}(t)$. Then, the epicardial strains in the principal direction can be computed from the eigenvalues ($\lambda_1(t)$, $\lambda_2(t)$) and the eigenvectors ($\rho_1(t)$, $\rho_2(t)$) of the tensor D(t).[1]

D. Local Wall Thickness and Regional Wall Stress

Under the assumption of the isochoric or volume preserving deformation, the third eigenvalue of the three-dimensional stretch tensor ($\lambda_3(t)$) must satisfy the following relationship[1],

$$\lambda_1(t) \cdot \lambda_2(t) \cdot \lambda_3(t) = 1 \tag{8}$$

The radial strain of regional myocardium ($\lambda_3(t)-1$) can be estimated from the epicardial strains ($\lambda_1(t)-1$, $\lambda_2(t)-1$). Then, the instantaneous regional wall thickness can be computed as,

$$h(t) = h_{ed}\, \lambda_3(t), \tag{9}$$

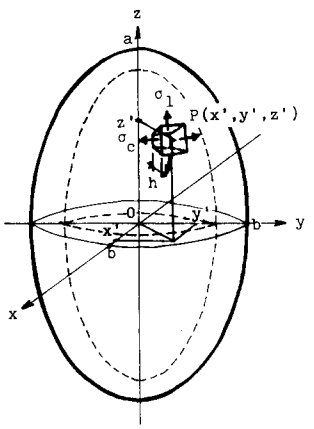

Fig. 2. Ellipsoidal model of the thick-walled left ventricle for the computation of the regional longitudinal (σ_1) and circumferential (c) wall stress of the cardiac wall segment at P (x', y', z').

where h_{ed} is the wall thickness at end-diastole.

We used a thick-walled left ventricular ellipsoidal model [11] as shown in Fig. 2 for computation of the longitudinal regional wall stress (σ_1) and the circumferential wall stress (σ_c) in the following equations. The derivation of these equations is summarized in the Appendix.

$$\rho_1 = \frac{P\, y'\, r}{h\,(h+2y')}, \qquad \rho_c = \frac{P}{h}\left[1 - \frac{(2r+h)\, y'\, r}{2Rr\,(h+2y')}\right] \frac{2Rr}{2R+h} \tag{10}$$

where a = base-to-apex semiaxis, b=minor semiaxis, P = left ventricular pressure, h = regional wall thickness as computed in Eq. (9),

$$r = \frac{(a^4 y'^2 + b^4 z'^2)^{1/2}}{a^2}$$

$$R = r^3 \frac{a^2}{b^4},$$

$$y' = \sqrt{(1 - f_z^2)} \cdot b, \text{ and } z' = f_z \cdot a \; (-1 < f_z < 1)$$

III. METHOD

A. Animal Preparation

The experiments were performed on four mongrel dogs weighing 25-34 kg. Each dog was anesthetized with intravenous pentobarbital sodium (10 mg/kg) and after intubation of endotracheal tube, ventilation was kept constant with a volume respirator (BENNETT PR-2) by oxygen and nitrous oxide. While the electrocardiogram was derived from the limb leads, the chest was opened through the left fifth intercostal space, the pericardium opened, and 4-8 markers were sutured to the epicardium in the vicinity of left coronary arterial bifurcations. The markers were made from lead shots, 1-2mm diameter. Without altering their relative position, we closed the chest and recovered the normal intrathoracic pressure with a water flask connected to a chest tube.

B. Coronary Cineangiography

The present algorithms for the regional myocardial motion were tested using the biplane coronary cineangiograms obtained in the marker implanted animal experiments and in the diagnostic evaluation of a patient's coronary circulation. The left ventriculogram and the left ventricular pressure waveforms were obtained with a catheter located in the left ventricle, used for injection of contrast medium and pressure measurement by Statham P23Db transducer. It was inserted through the femoral artery by the Seldinger technique and a bolus of radiopaque contrast media (Telebrix 60®) was injected using a power injector (Medrad, Mark IV) at an injection rate of 15ml/sec for a total amount of 45 ml. The electrocardiogram and left ventricular pressure were recorded using HP's 8-channel recording system (8890B). Then the catheter was located selectively in the coronary sinus for coronary angiography with a hand injection technique for total amount of 7ml, but in animal experiments aortography was performed due to difficulty in selection. After each injection of contrast media, a plastic plate of 15cm by 15cm with 100 pieces of 1mm lead shot was used for calibration of the biplane views of the angiograms for 1cm interdistance between the lead shots.

The angiographic system used in the present study consists of a X-ray generator (G.E., MSI-1250/v, 1000MA), image intensifier (9 in. circular, cesium iodide), plumbicon camera, and cinematograph (ARRITECHNO 35) with 35 mm film at the rate of 60 frames per second.

C. Data Collection

Using a vanguard 35 mm motion analyzer (XR-35), a HP Graphic Tablet (9111A), and DEC PDP-11/03 MINC microcomputer, each view of cineangiogram was digitized, and calibrated. The three-dimensional coordinate data were reconstructed to the fixed external camera coordinate system based upon the orthogonal projection. The three feature points were selected using the image of implanted lead markers and branch points of the coronary artery vessels as shown in Fig. 3. All data were collected within the first four beats after injection of contrast media.

Also, the recorded left ventricular pressure waveform and the electrocardiogram were digitized and used as input data for computation of the regional wall thickness and stress.

IV. RESULTS

A. Animal Experiment

Radiographic images of implanted markers in a experimental dog are shown in Fig. 3(a) and (b). Using these biplane angiograms, the perspective transformation technique of Eqs.

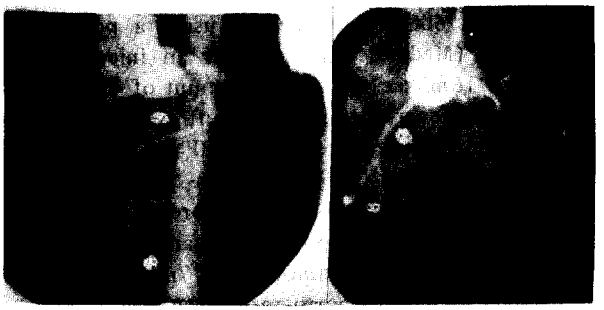

(a) (b)

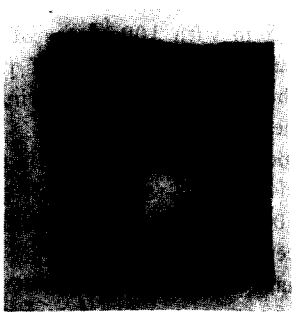

(c)

Fig. 3. An experimental dog's (# 4) cineangiograms with six implanted lead markers;
(a) RAO 30° view of the leaft anterior descending coronary artery with six implanted markers,
(b) LAO 60° view of the same vessel, and
(c) RAO 30° view of the left ventriculogram.

(3) and (4) was applied to the selected three feature points A,B,C corresponding to the lead markers or bifurcation points on the LAD branch. The same dog's left ventriculogram was used to obtain its major and minor axes during two consecutive heart cycle and wall thickness at the end-diastolic phase.

After the present regional epicardial deformation analysis, the local twist angle, $\alpha(t)$, was computed where the positive values of α shows the counter-clockwise rotation in Eq. (7). Using the stretch tensor's eigenvalues, the percentage changes of the epicardial strain was calculated as follows ;

$$\Lambda_1(t) = (\lambda_1(t) - 1) \times 100\,(\%) \qquad (11)$$
$$\Lambda_2(t) = (\lambda_2(t) - 1) \times 100\,(\%)$$

The local wall thickening was given as the strain in the radial direction ($\Lambda_3(t)$), as it was computed from the third eigenvalues of $\lambda_3(t)$ in Eq. (8) as follows;

$$\Lambda_3(t) = (\lambda_3(t) - 1) \times 100\,(\%) \qquad (12)$$

Then, using the least square error curve fitting method, a smoothed curve of the wall thickening was obtained. These computed parameters of local twist angle, epicardial shortenings, and regional wall thickening are shown in Fig. 4.

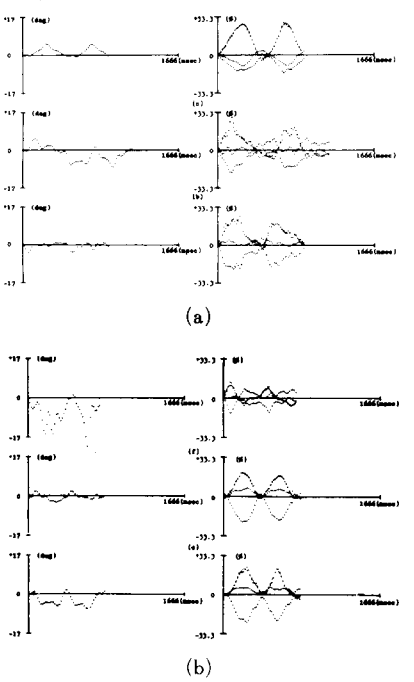

(a) (b)

Fig. 4. The left column shows the changes of the local twist angle, α. The right column shows the percentage changes of the epicardial shortening (Λ_1, Λ_2) and the radial thickening (Λ_3); Λ_1 at the bottom. Λ_2 in the middle, and Λ_3 at the top of each figure in the right column. Top four figures, (a), (b), (c), and (d), are obtained using coronary bifurcation points in L.V. base section for dogs, #1, #2, #3, and #4, respectively. These changes are also computed in dog # 4 using the implanted markers, as shown in (e) for base section and the apex region in (f). The similarity of the two methods can be shown in (d) and (e).

Using the measured left ventricular pressure, the regional wall stress was computed in Eq. (10) with f_z = 0.2, 0.5, and 0.9 for its locations of base, midwall, and apex section, respectively. Fig. 5. shows that the computed regional wall stress were greater for the circumferential direction than the longitudinal direction for all six cases.

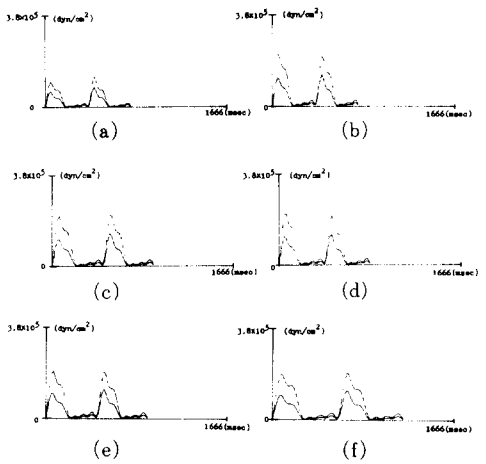

Fig. 5. Waveforms of the circumferential stress (upper) and longitudinal wall stress (lower) in LV. base section are shown in (a) – (d) for dogs #1 – #4, respectively, as computed using the coronary bifurcation points. The stress computed using the implanted markers are shown in (e) for the apex region, and (f) for L.V. base section in dog #4. The similarity of the results can be shown in (d) and (f) in the same region for the same subject.

B. Clinical Application

Fig. 6(a) and 6(b) show a normal patient's biplane coronary cineangiograms in RAO and LAO direction, respectively, and the three feature points were selected as the two bifurcation points and an inflection point on the LAD branch as shown in Fig. 6(a) and (b), with the same patient's left ventriculogram in Fig. 6(c). The time variation of the major axis, minor axis, and the left ventricular pressure are shown in Fig. 7(a), (b), and (c), respectively during two consecutive heart cycles. The end-diastolic pressure was 12 mmHg, and the peak systolic pressure was 140mmHg. As shown in

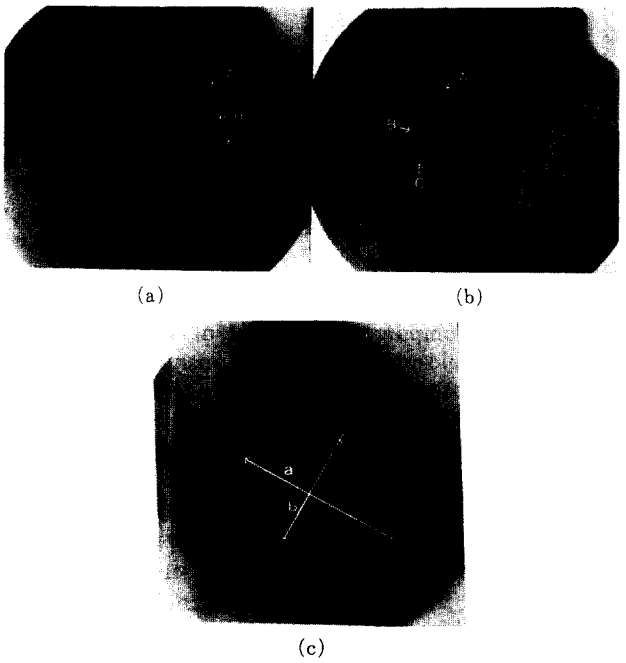

Fig. 6. A normal patienet's cineangiograms used for application of the present algorithm;
(a) RAO 30° view of the left anterior descending coronary artery with the three feature points A,B.C,
(b) LAO 60° view of the same vessel,
(c) RAO 30° view of the left ventricular chamber with major axis, minor axis, and wall thickness.

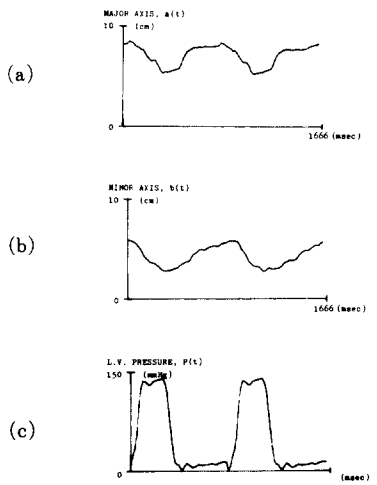

Fig. 7. Waveforms of the measured parameters of (a) major axis, (b) minor axis, and (c) left ventricular pressure.

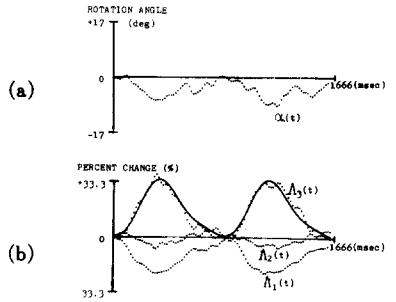

Fig. 8. Computed waveforms of the regional epicardial deformation analysis;
(a) local twist angle, $\alpha(t)$,
(b) percentage changes of the epicardial strains ($\Lambda_1(t)$, $\Lambda_2(t)$) and the radial strain ($\Lambda_3(t)$) with its fitted curve.

Fig. 8(a), the computed negative angle indicate that the local twist occurred with clockwise rotation, and the the local segment was shown to be rotated with its maximum value at the peak systolic pressure, and return slowly to the original position. In Fig. 8, the major shortening ($\Lambda_1(t)$) has a large change (22%) at the peak systolic pressure phase, and its waveform is shown to be similar to the measured changes of minor axis of Fig. 7(b). The maximum percentage changes of the local wall thickness was 37.8%.

The regional wall stress around the midwall section was computed using Eq. (10) with f_z = 0.3 for its location. As compared with the measured left ventricular pressure in Fig. 9,

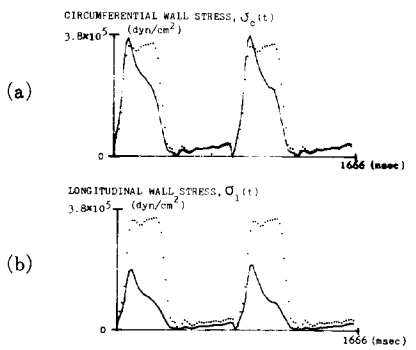

Fig. 9. Waveforms of the computed regional stress around the midwall section (f_z= 0.3);
(a) circumferential, and
(b) longitudinal wall stress.
The dotted curve shows the measured pressure changes.

the computed wall stress shows early diminution after its peak value while the left ventricular pressure continues to rise during the systolic phase. This observation is similar to the other reported results.[7] [9] [11]

The peak circumferential and longitudinal stresses were 3.79×10^5 and 2.06×10^5 (dyn/cm^2), respectively.

C. Simulation

Using Eq. (10), the regional stress at various points of the truncated ellipsoidal left ventricle was computed for the model of Fig. 10. In

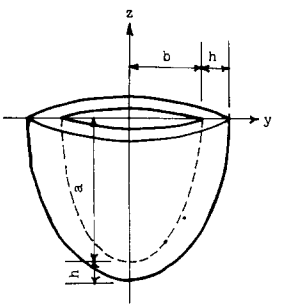

Fig. 10. Truncated ellipsoidal model of left ventricle used to simulate the regional stress at various points.

this computation, the measured left ventricular pressure, the major and minor semi-axes were used. Also, the wall thickness (h) was calculated by the following equation (14). For this analysis, the changes of the wall thickness were assumed to be same along the whole ventricle with the isochoric deformation at every instant during one heart cycle. Thus, it follows from these assumptions that,

$$\frac{4}{3}\pi\,[\,|a(t)+h(t)|^2\,|b(t)+h(t)|\,] - \frac{4}{3}\pi\,[a(t)^2 b(t)] = \text{constant.} \qquad (13)$$

Then, with the diastolic phase selected as a reference frame at t=0, the wall thickness h(t) must satisfy the following third order equation with respect to the time-varying constant parameters of a(t) and b(t) of the

major and minor semi-axes,

$$[h(t)^3+|2a(t)+b(t)|\,h(t)^2+|a(t)+2b(t)|\,a(t)h(t)] - [h(0)^3+|2a(0)+b(0)|\,h(0)^2+ +|a(0)+2b(0)|\,a(0)h(0)] = 0 \qquad (14)$$

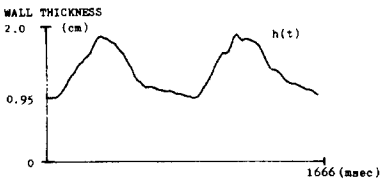

Fig.11. Waveforms of the wall thickness obtained under the assumption of the isochoric contraction during two heart cycles and used for the regional stress simulation.

A real solution of Eq. (14) was used as the wall thickness and is shown in Fig. 11. The distribution of the circumferential and longitudinal stresses from the base to apex were computed using these thickness data and are shown in Fig. 12. The result are similar to the previously reported distributions.[9]

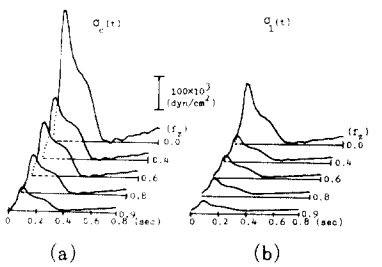

Fig. 12. Waveforms of the computed distribution of the (a) circumferential and (b) longitudinal wall stress from the base (f_Z=0.0) to apex (f_Z=1.0) of the truncated ellipsoidal left ventricle.

V. DISCUSSION

A new mathematical method was developed to estimate local epicardial deformation, wall thickness, and the regional wall stress using biplane coronary cineangiograms for four experimental dogs and a normal patient. Overall, consistent experimental results were obtained for the computed local twist angle, the regional wall thickening, the epicardial shortening, and the regional wall stress waveforms. There were some fluctuations and unperiodicity in dog # 1 and # 2, as shown in Fig. 4. These may be explained by the abnormality in ventricular function in these two dogs as caused by temporary arrest during the open heart surgery. Also, their regional wall stresses were shown to be reduced, compared with those of the dog # 3 and #4, as shown in Fig. 5.

The most significant results were obtained in dog #4, where all the computed waveforms obtained from coronary arterial bifurcation points data are highly correlated with those from lead markers position data, as shown in Fig. 4(d) and (e). This result supports the basic assumption of the present algorithm that the coronary arterial bifurcation points can be used as the landmarks of the epicardial motion.

Also, the results show that there are significant difference in the computed stress and strain depending upon the locations of the three feature points. The apex section of the left ventricle contracts in the earlier systolic phase and rotate more than the base section, as shown in Fig. 4(e) and (f). The regional wall stresses in the apex are smaller than those in the base region, as shown in Fig. 5(e) and (f).

Our study presents a new analytical method of utilizing two previous studies; one is that the bifurcations of coronary arteries can provide natural landmarks of the epicardial surface changes, and the other result showed that the motion image of the markers can be used for computing the regional wall deformation.[3][11]

Thus, the objective of the present study was to increase clinical utilization of coronary angiography by providing myocardial informations including regional stress distribution. Previously, due to the difficulties in measuring the regional changes of wall thickness using conventional left ventriculograms or echocardiograms, it was difficult to calculate the regional wall stress[12] In the present study, the biplane image analysis method was developed to estimate the regional stress with

less complexities than the previous methods, but the estimation results show its validity of the present method, as compared with the previous results [9].

Because our model is based upon the geometric assumption of left ventricle as an ellipsoid of revolution, the calculated stresses provides its values under the condition that the same stress was developed at any point on the cross-sectional plane perpendicular to the major axis. Therefore, only one parameter, f_z, in Eq. (10), which is a position factor of a specific cross-section on the major axis, is necessary to locate the region of interest on the ellipsoid.

The present algorithm has several advantages for the clinical applications: First, the regional changes of deformation and wall stress of myocardium can be achieved after elimination of the global effects. These have been difficult to obtain in the conventional methods. Second, the data collection is relatively easy, and the procedure is safer than any other method including the marker implantation method, which was thought to be the most reliable technique for estimation of epicardial motion. Third, the clinical evaluation of these regional myocardial changes together with the deficiency of the blood supply in one diagnostic procedure may be very useful for early detection of the impaired region around the coronary arteries. Also, it may be useful to evaluate the clinical significance of the region with normal wall stress while the region is supplied with the narrowed blood vessels.

Our technique has the following possible limitations: First, any sliding effects between the bifurcation points and the myocardium may exist depending upon the degree of coupling, and it must be considered. While a close correlation was reported [3] between the position data of the bifurcations and the metal markers points, other feature points, such as inflection points, may affect the results. With improved image quality of the biplane coronary cineangiogram, these problems can be avoided by using only the bifurcation points for analysis. Second, when the blood supply is severely obstructed due to arterial occlusion, the tracing of the feature points around the region will be difficult. Third we must also consider the effects of the contrast medium on the contractility, while the previous results showed that the diminsional changes of the epicardial segment were not affected by intracoronary injection of contrast medium less than 25ml in the first 5 to 6 cardiac cycles.[3] [4]

In conclusion, the present method provides a new technique of evaluating the regional wall deformation and wall stress together with the blood vessel conditions in a single coronary cineangiography procedure.

APPENDIX

Calculation of the regional stress of a thick ellipsoid of revolution.

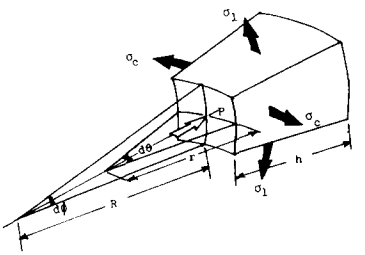

Fig.13. A thick-walled left ventricular wall segment with the principal radii of curvature R and r.

Laplace's law for a thick-walled shell as shown in Fig. 13 may be written in terms of two stress components, σ_c and σ_1 [11];

$$\frac{P}{h} = \frac{2R+h}{2Rr}\sigma_c + \frac{2r+h}{2Rr}\sigma_1 \qquad (A1)$$

where r and R are the principal radii of curvature, σ_c and σ_1 are the circumferential and longitudinal stress components, respectively, P is left ventricular pressure, and h is the regional wall thickness. If the wall is thin, Eq. (A1) reduces to the Sandler and doge's equation [7];

$$\frac{P}{h} = \frac{\sigma_c}{r} + \frac{\sigma_1}{R} \qquad (A2)$$

In Eq. (A1), to determine absolute values of each stress at a specific point, three para-

meters (r, R, and σ_c (or σ_1)) must be known in addition to P and h. The principal radii of curvature at any point on an ellipsoid of revolution with the general form such as,

$$b^2x^2 + b^2y^2 + a^2z^2 = a^2b^2, \qquad (A3)$$

where a and b are major and minor semi-axial lengthes, respectively, and the major axis is on the z axis, can be represented as [13];

$$R = r^3\frac{a^2}{b^4}, \quad r = \frac{(a^4y^2 + b^4z^2)^{1/2}}{a^2} \qquad (A4)$$

For a point at the equator of the ellipsoid, Eq. (A4) can be redued to,

$$R = \frac{a^2}{b}, \quad r = b. \qquad (A5)$$

From now on, we will consider the elliptical points on x=0 plane, i.e. y-z plane, for simplicity of analysis without losing the generality because of symmetricity of the ellipsoid of revolution. In this case, the ellipse on y-z plane is represented as shown in Fig. 14(a),

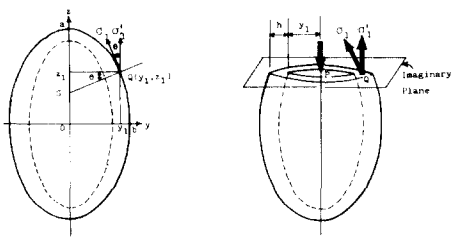

(a) (b)

Fig.14 Thick-walled ellipsoidal model of left ventricle;
(a) relationship between the stress components in the two-dimensional plane, and
(b) total force balance condition between the pressure in the cavity and wall stress on the cross-sectional imaginary plane.

$$\frac{y^2}{b^2} + \frac{z^2}{a^2} = 1, \qquad (A6)$$

and the coordinates of an arbitrary point Q (y_1, z_1) can be located with a fraction f_z,

$$z_1 = f_z \cdot a \quad (-1 < f_z < 1) \qquad (A7)$$

$$y_1 = f_y \cdot b = \sqrt{(1-f_z^2)} \cdot b$$

Then, using simple geometric calculations of two-dimensional ellipse, one can determine the longitudinal stress σ_1 at a point Q. From Fig. 14(b), the total force balance condition between the pressure in the cavity and wall stress on the cross-sectional imaginary plane which includes the point Q and perpendicular to the major axis, must be satisfied as [14],

$$P\cdot\pi\cdot y_1^2 = \sigma_1' \pi [(y_1+h)^2 - y_1^2],$$

$$\text{or} \quad \sigma_1' = \frac{P\ y_1^2}{h(2y_1+h)}, \qquad (A8)$$

where y_1 is given in Eq. (A7) and σ_1' is the vertical component of σ_1 and other parameters are as defined above. Using the equation of normal line SQ at point Q in Fig. 14(a), the geometric relation between σ_1 and σ_1' can be represented as,

$$\sigma_1 = \sigma_1' / \cos\theta, \qquad (A9)$$

$$\text{where} \quad \cos\theta = \frac{a^2\ y_1}{(a^4y_1^2 + b^4z_1^2)^{1/2}} = \frac{y_1}{r}$$

From Eqs. (A8) and (A9), the longitudinal stress at a point Q is given by,

$$\sigma_1 = \frac{P\ y_1\ r}{h\ (h + 2y_1)} \qquad (A10)$$

Then, the circumferential stress σ_c at a point $Q(y_1, z_1)$ can be determined from the Eq. (A1) and Eq. (A10),

$$\sigma_c = \frac{P}{h}\left\{1 - \frac{(2r+h)\ y_1 \cdot r}{2Rr\ (h+2y_1)}\right\}\frac{2Rr}{2R+h}, \qquad (A11)$$

where all parameters are defined previously.

REFERENCES

[1] G.D. Meier, M.C. Ziskin, W.P. Santamore, and A.A. Bove, "Kinematics of the beating heart," *IEEE Trans. Biomed. Eng.*, vol. BME-27, no. 6, pp. 319-329, June 1980.

[2] K.R. Walley, M. Grover, G.L. Raff, J.W. Benge, B. Hannaford, and S.A. Glantz, "Left ventricular dynamic geometry in the intact and open chest dog," *Circ. Res.*, vol. 50, pp. 573-589, 1982.

[3] Y. Kong, J.J. Morris, and H.D. McIntosh, "Assessment of regional myocardial performance from biplane coronary cineangiograms," *Am. J. of Cardio.*, vol. 27, pp. 529-537, 1971.

[4] M.J. Potel, J.M. Rubin, S.A. MacKay, A.M. Aisen, J. Al-Sadir, and R.E. Sayre, "Methods for evaluating cardiac wall motion in three dimensions using bifurcation points of the coronary arterial tree," *Invest. Radiol.*, vol. 18, pp. 47-57, 1983.

[5] H.C. Kim, B.G. Min, T.S. Lee, S.J. Lee, C.W. Lee, J.H. Park, and M.C. Han, "Three-dimensional digital subtraction angiography," *IEEE Trans. Med. Imag.*, vol. MI-1, no. 2, pp. 152-158, Oct. 1982.

[6] P.A. McHale, and J.C. Greenfield, "Evaluation of several geometric models for estimation of left ventricular circumferential wall stress," *Circ. Res.*, vol. 33, pp. 303-312, Sept 1973.

[7] H. Sandler and H.T. Dodge, "Left ventricular tension and stress in man," *Circ. Res.*, vol. 13, pp. 91-104, 1963.

[8] P.S. Laplace, *Theorie de laction capillaire.* In Traite de Mecanique Celeste, Supplement au livre 10, Paris, Couroien, 1805.

[9] A.Y.K. Wong and P.M. Rautaharju, "Stress distribution within the left ventricular wall approximated as a thick ellipsoidal shell," *Am. Heart J.*, vol. 75, pp. 649-662, 1968.

[10] I. Mirsky, "Left ventricular stresses in the intact human heart," *Biophys. J.*, vol. 9, pp. 189, 1969.

[11] H.L. Falsetti, R.E. Mates, C. Grant, D.G. Greene, and I.L. Bunnell, "Left ventricular wall stress calculated from one-plane cineangiography. – An approach to force-velocity analysis in man," *Circ. Res.*, vol. 26, pp. 71-83, Jan. 1970.

[12] W.P. Hood Jr., W.J. Thomson, C.E. Rackley, and E.L. Rolett, "Comparison of calculations of left ventricular wall stress in man from thin-walled and thick-walled ellipsoidal models," *Circ. Res.*, vol. 24, pp. 575-582, Apr. 1969.

[13] S. Timoshenko, *Theory of plates and shells. ed. 2, New York,* McGraw-Hill Book Company Inc., pp. 440, 1959.

[14] L.L. Hefner, L.T. Sheffield, G.C. Cobbs, and W. Klip, "Relation between mural force and pressure in the left ventricle of the dog," *Circ. Res.*, vol. 11, pp. 654-663, Oct. 1962.